American Mineralogist, Volume 99, pages 1802–1805, 2014

LETTER

Crystal chemistry of dense hydrous magnesium silicates: The structure of phase H, $MgSiH_2O_4$, synthesized at 45 GPa and 1000 °C

LUCA BINDI[1,2,*], MASAYUKI NISHI[3,4], JUN TSUCHIYA[3,4] AND TETSUO IRIFUNE[3,4]

[1]Dipartimento di Scienze della Terra, Università di Firenze, Via La Pira 4, I-50121 Firenze, Italy
[2]CNR, Istituto di Geoscienze e Georisorse, sezione di Firenze, Via La Pira 4, I-50121 Firenze, Italy
[3]Geodynamics Research Center, Ehime University, Matsuyama 790-8577, Japan
[4]Earth-Life Science Institute, Tokyo Institute of Technology, Tokyo 152-8550, Japan

ABSTRACT

The crystal structure of the dense hydrous magnesium silicate phase H, $MgSiH_2O_4$, synthesized at 45 GPa and 1000 °C, was investigated by single-crystal X-ray diffraction. Although showing a deterioration process under the X-ray beam, the compound was found to be orthorhombic, space group *Pnnm* ($CaCl_2$-type structure), with lattice parameters $a = 4.733(2)$, $b = 4.3250(10)$, $c = 2.8420(10)$ Å, $V = 58.18(3)$ Å^3, and $Z = 1$. The structure was refined to $R_1 = 0.0387$ using 53 observed reflections [$2\sigma(I)$ level]. Magnesium and silicon were found to be disordered at the same octahedral site (with a mean bond distance of 1.957 Å). Hydrogen was not located in the difference Fourier maps, but it is very likely disordered at a half-occupied 4*g* position. The centrosymmetric nature of the structure of phase H is examined in relation to that reported for pure δ-AlOOH at ambient conditions (non-centrosymmetric, $P2_1nm$), and the possibility that these two compounds can form a solid solution at least at high pressure is discussed.

Keywords: Phase H, dense hydrous magnesium silicates, lower mantle, crystal structure, synthesis

INTRODUCTION

Dense hydrous magnesium silicates (DHMS) play an important role in the transportation of water into the deep mantle by the subduction of oceanic slabs. Until recently, phase D has been considered to be the highest pressure form of DHMS (Frost and Fei 1998; Shieh et al. 1998). However, Tsuchiya (2013) and Nishi et al. (2014) found that phase D transforms to a new dense hydrous silicate, phase H, at pressures above ~48 GPa. Phase H in the descending slab may deliver a significant amount of water to the deepest part of the lower mantle thus influencing the structure and dynamics of the deep mantle.

On the basis of an in situ energy-dispersive X-ray diffraction study Nishi et al. (2014) found that the reflections of phase H at ambient conditions could be indexed with an orthorhombic cell with $a \approx 4.7$, $b \approx 4.3$, $c \approx 2.8$ Å. However, the quality of the collected X-ray diffraction patterns was insufficient to allow the detailed structure of phase H to be reliably determined (see Nishi et al. 2014). Therefore, these authors limited their study to report either $P2_1nm$ (by analogy with the δ-AlOOH structure; Suzuki et al. 2000; Komatsu et al. 2006) or $P2/m$ (as inferred from theoretical calculations; Tsuchiya 2013) as possible space groups, with a preference for the orthorhombic symmetry. Electron diffraction measurements with a transmission electron microscope also failed to obtain the structural data because of rapid amorphization of the sample during observations. To determine the detailed structure of phase H, different techniques in the analyses of the recovered sample are required.

Here we report the results of a structural study of phase H by single-crystal X-ray diffraction on fragments directly extracted from the run products synthesized at 45 GPa and 1000 °C. The structure and the space group of phase H have been unequivocally identified and considerations on the possible $MgSiH_2O_4$–$AlAlH_2O_4$ solid solution at high pressures are reported.

EXPERIMENTAL METHODS

Synthesis

Synthesis experiments were conducted using a 1500-t multi-anvil apparatus (MADONNA-II) at Ehime University (Matsuyama, Japan). We used sintered diamond anvils with a truncated edge length of 1.5 mm as the second-stage anvils. The sample was loaded into a gold capsule. The sample assembly was composed of sintered (Mg,Cr)O and MgO pressure media, with a cylindrical $LaCrO_3$ heater, and a molybdenum electrode. Temperature was monitored by a $W_{97}Re_3$-$W_{75}Re_{25}$ thermocouple. The pressure media and a heater were dried at 1000 °C for 3 h before assembling the high-pressure cell. Details of the sample assembly are shown in the supplementary information by Nishi et al. (2014). We used the $MgSiH_2O_4$ composition as starting material, which is prepared from $Mg(OH)_2$ brucite and SiO_2 silica powders in a 1:1 molar ratio.The sample was compressed to 45 GPa at room temperature. Then the temperature was increased to 1000 °C and held constant for 6 h. Phase H prevailed in the run product, being accompanied by trace amounts of $MgSiO_3$ perovskite (Fig. 1).

Strategy for the X-ray data collection

Two crystals were hand-picked under a reflected light microscope from the run product MII201H (Fig. 1), mounted on a 0.008 mm diameter carbon fiber and examined with an Oxford Diffraction Xcalibur 3 diffractometer (X-ray Mo$K\alpha$ radiation, $\lambda = 0.71073$ Å) equipped with a Sapphire 2 CCD detector. After some minutes of X-ray exposure, intensity decrease and broadening of the reflections belonging to phase H were observed. Such an intensity decay of phase H during the data collection was attributed to a progressive amorphization process. Under the electron beam, the amorphization was quite immediate (Nishi et al. 2014). Under the X-ray beam, the process was slower, but, in the end (after ~140 min), a total disappearance of the reflections was noticed. However, the unit-cell parameters obtained for the first two crystals of phase H using the very low number of collected reflections

* E-mail: luca.bindi@unifi.it

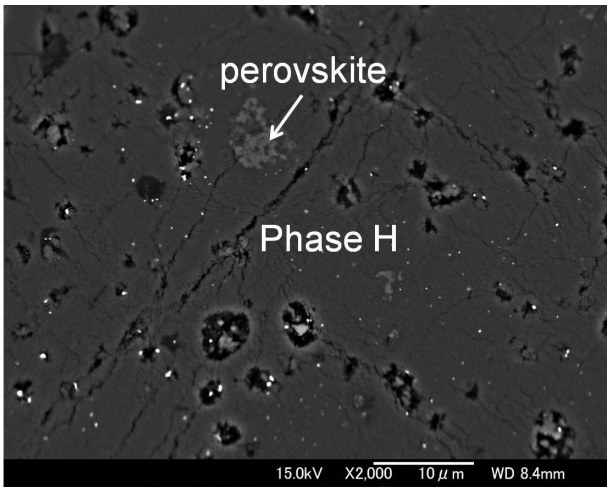

FIGURE 1. Backscattered electron image of the run product MII201H synthesized at 45 GPa and 1000 °C. White small dots are the gold derived from capsule. Scale bar is indicated.

yielded an orthorhombic cell with $a \approx 4.7$, $b \approx 4.3$, $c \approx 2.8$ Å, in agreement with the observations of Nishi et al. (2014) at ambient conditions.

At this point, a third small crystal (24 × 35 × 41 μm) was selected and tested taking into account the observed deterioration process (see Table 1 for details). The crystal was found to be composed of approximately 95% phase H and 5% gold. Trace amounts of perovskite (Fig. 1) were not detected. The deterioration of phase H was estimated by careful measurements of selected strong reflections belonging to phase H (i.e., 110, 011, and 121) with reference to the strong 220 reflection belonging to the Au structure (which does not show interferences with the reflections of phase H). In other words, gold was used as internal standard (as this material does not undergo the deterioration process), and the frames where these reflections occurred (Fig. 2) were collected 21 times during the entire data collection. The Ewald sphere was collected up to $\theta_{max} \approx 27°$ with 99.8% completeness, which is a very satisfactory result given the observed deterioration and the size of the crystal. The number of independent reflections was sufficient both to identify the correct space group and begin the structure determination (see below).

Intensity integration and standard Lorentz-polarization corrections were done with the CrysAlis RED (Oxford Diffraction 2006) software package. The program ABSPACK of the CrysAlis RED package (Oxford Diffraction 2006) was used for the absorption correction.

RESULTS AND DISCUSSION

Space group determination and structure solution

The orthorhombic unit-cell values obtained for phase H using only the X-ray reflections collected in the first 60 min (to avoid the use of reflections affected by deterioration effects) are a = 4.733(2), b = 4.3250(10), c = 2.8420(10) Å. No deviation from 90° was observed by refining the unit cell without symmetry constraints. The observed reflection conditions are the following: 0kl: k+l = 2n, h0l: h+l = 2n, h00: h = 2n, 0k0: k = 2n, and 00l: l = 2n, thus leading to the choice of *Pnnm* or *Pnn*2 as possible space groups. The statistical tests on the distribution of |E| values ($|E^2 - 1| = 0.952$) strongly indicated the presence of an inversion center, thus suggesting the choice of the space group *Pnnm*. The position of the cation (Mg/Si) was determined by means of direct methods (Sheldrick 2008). A least-squares refinement on F^2 using this position and isotropic temperature factor produced an R_1 factor of 0.074. Three-dimensional difference Fourier synthesis yielded the position of the remaining oxygen atom. The program SHELXL (Sheldrick 2008) was used for the refinement of the structure. The occupancy of the cation site was left free to vary (Si vs. vacancy) and led to an electron number of 12.94(8). Such a value is very close to a $Mg_{0.50}Si_{0.50}$ site population (mean electron number = 13) and thus, to reduce the number of free variables, the occupancy was fixed to this distribution. Neutral scattering curves for Mg, Si, and O were taken from the *International Tables for X-ray Crystallography* (Ibers and Hamilton 1974). At this point, a careful examination of the difference Fourier maps (ΔF), did not allow the precise location for the H atom. Notwithstanding, the first peak in the ΔF (0.64 e^- Å^{-3}) was at coordinates 0.475, 0.042, 0 (Wyckoff position 4*g*), at about 1.0 Å from the oxygen atom, but it was not included in the refined model. At the last stage, with isotropic atomic displacement parameters for all atoms, the residual value settled at R_1 = 0.0387 for 53 observed reflections [2σ(I) level] and 5 parameters and at R_1 = 0.0729 for all 73 independent reflections. The ratio between the number of observed reflections and the refined parameters is adequate (53/5 = 10.6).

TABLE 1. Data and experimental details for the selected crystal

Crystal data	
Formula	$MgSiH_2O_4$
Crystal size (mm)	0.024 × 0.035 × 0.041
Form	block
Color	transparent
Crystal system	orthorhombic
Space group	*Pnnm* (#58)
a (Å)	4.733(2)
b (Å)	4.3250(10)
c (Å)	2.8420(10)
V (Å^3)	58.18(3)
Z	1
Data collection	
Instrument	Oxford Diffraction Xcalibur 3
Radiation type	Mo$K\alpha$ (λ = 0.71073)
Temperature (K)	298(3)
Detector to sample distance (cm)	6
Number of frames	314
Measuring time (s)	30
Maximum covered 2θ (°)	52.87
Absorption correction	multi-scan (ABSPACK; Oxford Diffraction 2006)
Collected reflections	510
Unique reflections	73
Reflections with $F_o > 4\sigma(F_o)$	53
R_{int}	0.0312
Range of h, k, l	$-5 \le h \le 5$, $-5 \le k \le 5$, $-3 \le l \le 3$
Refinement	
Refinement	Full-matrix least squares on F^2
Final R_1 [$F_o > 4\sigma(F_o)$]	0.0387
Final R_1 (all data)	0.0729
Number of least-squares parameters	5
$\Delta\rho_{max}$ (e Å^{-3})	0.64
$\Delta\rho_{min}$ (e Å^{-3})	–0.53

The calculated X-ray powder-diffraction pattern, computed with the atomic coordinates and occupancies obtained in this study (Table 2), is given in Table 3 together with the measured pattern obtained by Nishi et al. (2014) at 42 GPa and 1000 °C. Table 4[1] lists the observed and calculated structure factors.

Description of the structure

The structure of phase H was found to be topologically identical to that of $CaCl_2$ (Fig. 3). The tetragonal symmetry of

[1] Deposit item AM-14-815, Table 4 and CIF. Deposit items are stored on the MSA web site and available via the *American Mineralogist* Table of Contents. Find the article in the table of contents at GSW (ammin.geoscienceworld.org) or MSA (www.minsocam.org), and then click on the deposit link.

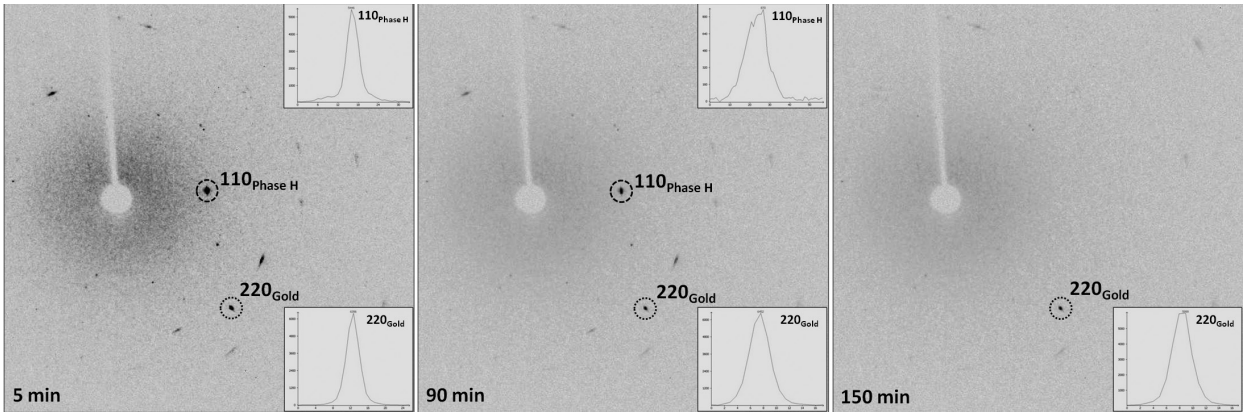

FIGURE 2. A frame showed in different moments of the data collection (after 5, 90, and 150 min, respectively) evidencing the progressive broadening and decrease of intensity of the reflections belonging to phase H. The insets in the first two panels refer to the diffraction profile of a reflection belonging to phase H (up) and a reflection belonging to the gold structure (down). In the last panel (right), no reflections belonging to phase H are present, thus indicating the total amorphization of the compound.

TABLE 2. Fractional atomic coordinates, site occupancy factors (s.o.f.), isotropic displacement parameters (Å^2) and geometric parameters (Å, Å^3, °) for phase H

	s.o.f.	*x*	*y*	*z*	U_{iso}
M	$Mg_{0.50}Si_{0.50}$	0.0000	0.0000	0.0000	0.013(1)
O	$O_{1.00}$	0.347(1)	0.230(1)	0.0000	0.018(2)
H[a]	$H_{0.50}$	0.475	0.042	0.0000	
M–Oi	1.922(5)		$O^{ii,iii,iv,v}$–M–$M^{vi,vii}$		136.0(1)
M–O	1.922(5)		$O^{ii,iii,iv,v}$–M–$M^{vi,vii}$		44.0(1)
M–Oii	1.975(4)		O^{i}–M–M^{ix}		153.74(7)
M–$O^{i,ii}$	1.975(4)		O–M–M^{ix}		26.26(7)
M–O^{iv}	1.975(4)		O^{ii}–M–M^{ix}		114.1(2)
M–O^{v}	1.975(4)		O^{iii}–M–M^{ix}		80.0(2)
<M–O>	1.957		O^{iv}–M–M^{ix}		65.9(2)
σ^2	1.474		O^{v}–M–M^{ix}		100.0(2)
λ	1.0008		M^{vi}–M–M^{ix}		66.094(9)
V	10.0		M^{vii}–M–M^{ix}		113.906(9)
M–$M^{vi,v,ii}$	2.842(1)				
M–$M^{viii,ix}$	3.5066(8)				
O^{i}–M–O	180.0(3)		O–H		1.01
O^{i}–M–$O^{ii,iii,iv,v}$	90.40(7)		H–O		1.45
O–M–$O^{ii,iii,iv,v}$	89.60(7)		O···O		2.461(4)
$O^{ii,iv}$–M–$O^{iii,v}$	92.0(2)		O–H–O		178.9
$O^{ii,iii}$–M–$O^{iv,v}$	180.0(4)				
$O^{ii,iii}$–M–$O^{iv,v}$	88.0(2)				

[a] Assuming the atom coordinates of the first peak in the Δ*F* as those of the H atom (in agreement with Komatsu et al. 2011) and a 50% occupancy. Symmetry codes: (i) −*x*, −*y*, −*z*; (ii) −*x*+1/2, *y*−1/2, −*z*−1/2; (iii) −*x*+1/2, *y*−1/2, −*z*+1/2; (iv) *x*−1/2, −*y*+1/2, *z*+1/2; (v) *x*−1/2, −*y*+1/2, *z*−1/2; (vi) *x*, *y*, *z*+1; (vii) *x*, *y*, *z*−1; (viii) −*x*−1/2, *y*−1/2, −*z*−1/2; (ix) −*x*+1/2, *y*+1/2, −*z*+1/2. Quadratic elongation (λ) and angle variance (σ^2) calculated according to Robinson et al. (1971).

TABLE 3. X-ray powder diffraction patterns for phase H

1			2		
hkl	d_{calc} (Å)	I_{calc}	*hkl*	d_{obs} (Å)	I/I_o
110	3.1928	100	110	3.021	100
101	2.4365	5	101	2.314	7
011	2.3751	81	011,200	2.250	overlap gold
200	2.3665	12			
111	2.1228	69	111	2.012	73
210	2.0760	41	210	1.967	45
211	1.6764	34	211	1.589	23
121	1.6174	73	121	1.531	24
220	1.5964	27	220	1.510	12
310	1.4821	13	310	1.403	14
002	1.4210	18	002	1.350	8
301	1.3794	29	301,130	1.308	10
130	1.3791	12			
112	1.2982	11	112	1.231	2
131	1.2407	5	–	–	–
212	1.1726	5	–	–	–
231	1.1297	10	–	–	–
040	1.0812	5	–	–	–
222	1.0614	11	–	–	–
411	1.0591	6	–	–	–
420	1.0380	8	–	–	–
312	1.0257	7	–	–	–
132	0.9897	7	–	–	–

Notes: 1 = calculated powder pattern and indexing for phase H of this study. *d* values calculated on the basis of *a* = 4.733(2), *b* = 4.325(1), *c* = 2.842(1) Å, and with the atomic coordinates and occupancies given in Table 2. Intensities calculated using XPOW software version 2.0 (Downs et al. 1993). 2 = observed powder pattern (collected at 42 GPa and 1000°C) and indexing originally reported by Nishi et al. (2014).

the rutile-type structure is broken by the mutual rotation of the strands of octahedra. The cations (Mg and Si) were found to be disordered at the origin of the unit cell (Wyckoff position 2*a*), whereas the oxygen atom was found to be in a 4*g* position (Table 2). The mean octahedral metal-oxygen distance of 1.957 Å is in good agreement with the calculated value for $^{VI}[Mg\text{-}O]_{0.50}$ + $^{VI}[Si\text{-}O]_{0.50}$ of 1.94 Å (taking into account the ionic radii; Shannon 1976) and that obtained considering the average octahedral bond value of MgO_6 and SiO_6 polyhedra in the structure of $MgSiO_3$ ilmenite (1.94 Å; Horiuchi et al. 1982). Interestingly, Komatsu et al. (2011), by means of neutron diffraction studies at ambient conditions, found that the Tschermak $Si^{4+} + Mg^{2+} \leftrightarrow 2Al^{3+}$ substitution does not induce either an enlargement of the orthorhombic unit cell [V = 56.375(1) and 56.217(1) Å^3 for δ-AlOOH and δ-$(Al_{0.86}Mg_{0.07}Si_{0.07})OOH$, respectively] or a lengthening of the octahedral bond distances (1.923 and 1.922 Å, respectively). On the contrary, we noticed a considerable increase of the unit-cell volume [58.18(3)] and of the M-O distance (1.957 Å) passing from the pure Al- to the (MgSi)-compound.

The quality of the diffraction data did not allow the determination of the hydrogen atom position with confidence. However, the first peak in the Δ*F* was at coordinates 0.475, 0.042, 0 (Wyckoff position 4*g*), and this position is in excellent agreement with that found by Komatsu et al. (2011) for the *Pnnm* structure of δ-$(Al_{0.86}Mg_{0.07}Si_{0.07})OOH$ [i.e., 0.4835(11), 0.0401(9), 0]. If we assume that the position found for hydrogen in phase H is real

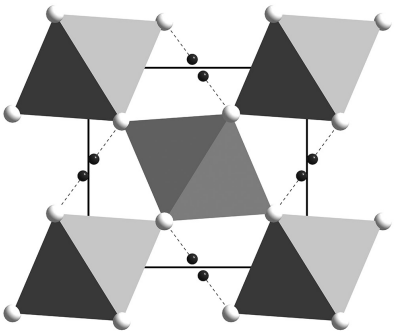

FIGURE 3. The crystal structure of phase H down [001]. The horizontal direction is the *a* axis. Gray polyhedra refer to (Mg,Si)-O octahedra; white circles refer to oxygen atoms, whereas the hydrogen atoms (small black circles) have been tentatively drawn at the Wyckoff position 4*g* (0.475, 0.042, 0) and bonded (dashed lines) to oxygen. The fact that hydrogen is half occupied does impede the formation of the unrealistic H–H distance of 0.43 Å.

(with a 50% occupancy), the following hydrogen bonding system is obtained: O–H = 1.01 Å, H–O = 1.45 Å, O···O = 2.461(4) Å, and O–H–O = 178.9°.

Considerations on the $MgSiH_2O_4$–$AlAlH_2O_4$ join

We have here demonstrated that phase H retains its centrosymmetricity (being derived from the original rutile-type structure) and that it crystallizes with the $CaCl_2$-type structure, *Pnnm* space group. The previously inferred space group, $P2_1nm$, cannot be assumed because of the presence of additional systematic absences (i.e., 0*kl*: $k+l = 2n+1$ and 0*k*0: $k = 2n+1$) beside those typically due to that space group. The non-centrosymmetric *Pnn*2 space group has to be discarded as well, since there is no structural reasons to remove the inversion center. Analogously, Komatsu et al. (2011) pointed out that the *Pnnm* model is more appropriate than the *Pnn*2 model previously reported (Kudoh et al. 2004) to describe the structure of δ-$(Al_{0.86}Mg_{0.07}Si_{0.07})OOH$. This is because it is unlikely that the ordering of the minor Mg/Si cations substituting for Al along the *c* axis causes the loss of the mirror plane perpendicular to *c* axis. The main reason for the eventual breaking of the mirror plane would be represented by the desymmetrization of the H atom position. However, no split H positions were observed by Komatsu et al. (2011) for δ-$(Al_{0.86}Mg_{0.07}Si_{0.07})OOH$, and the previous *Pnn*2 model reported by Kudoh et al. (2004) was found to be identical to a centrosymmetric description of the structure (see discussion in Komatsu et al. 2011).

The only reasonable decrease of symmetry for the structure of phase H would be toward the monoclinic subgroup *P*2/*m*, which would allow the ordering of Mg and Si into two different octahedra (Tsuchiya 2013). However, this model seems unlikely at least at ambient conditions or at high *P*-*T* because it would imply a distortion giving rise to a monoclinic β angle different from 90° (i.e., 93°; Tsuchiya 2013) and, more importantly, would lead to an increase of diffraction lines in the powder pattern not observed in either synchrotron X-ray powder diffraction experiments (Nishi et al. 2014) or by single-crystal investigations (this study).

The crystal structure of pure δ-AlOOH has been proved to be non-centrosymmetric, space group $P2_1nm$ (Komatsu et al. 2006). The presence of Mg and Si substituting for Al (even in very low amounts) was observed to provoke the $P2_1nm \rightarrow Pnnm$ transition (Komatsu et al. 2011). We have here demonstrated that phase H, with pure $MgSiH_2O_4$ stoichiometry, crystallizes in the *Pnnm* space group. Thus, it seems that when cations with different valence states (i.e., Mg^{2+}, Al^{3+}, and Si^{4+}) become disordered at the octahedral sites, a fluctuation of the hydrogen positions occurs to keep the charge neutrality. Such a disordered distribution of hydrogen is considered the crystallographic breaker for the symmetry change (Komatsu et al. 2011). These considerations, together with the fact that the structure of pure δ-AlOOH was found to undergo a phase transition to *Pnnm* at $P > 8$–9 GPa (Sano-Furukawa et al. 2008; Kuribayashi et al. 2014), imply that $MgSiH_2O_4$ and $AlAlH_2O_4$ could form a complete solid solution at high pressure, likely acting therefore as a fundamental water reservoir in the deep mantle.

ACKNOWLEDGMENTS

The manuscript improved thanks to Ian Swainson and three anonymous reviewers. The research was supported by "progetto di Ateneo 2012, University of Firenze" to L.B., by C.N.R., Istituto di Geoscienze e Georisorse sezione di Firenze, Italy.

REFERENCES CITED

Downs, R.T., Bartelmehs, K.L., Gibbs, G.V., and Boisen, M.B. Jr. (1993) Interactive software for calculating and displaying X-ray or neutron powder diffractometer patterns of crystalline materials. American Mineralogist, 78, 1104–1107.

Frost, D.J., and Fei, Y. (1998) Stability of phase D at high pressure and high temperature. Journal of Geophysical Research, 103, 7463–7474.

Horiuchi, H., Hirano, M., Ito, E., and Matsui, Y. (1982) $MgSiO_3$ (ilmenite-type): single crystal X-ray diffraction study. American Mineralogist, 67, 788–793.

Ibers, J.A., and Hamilton, W.C., Eds. (1974) International Tables for X-ray Crystallography, vol. IV, 366p. Kynock, Dordrecht, The Netherlands.

Komatsu, K., Kuribayashi, T., Sano, A., Ohtani, E., and Kudoh, Y. (2006) Redetermination of the high-pressure modification of AlOOH from single-crystal synchrotron data. Acta Crystallographica, E, 62, i216–i218.

Komatsu, K., Sano-Furukawa, A., and Kagi, H. (2011) Effects of Mg and Si ions on the symmetry of δ-AlOOH. Physics and Chemistry of Minerals, 38, 727–733.

Kudoh, Y., Kuribayashi, T., Suzuki, A., Ohtani, E., and Kamada, T. (2004) Space group and hydrogen sites of δ-AlOOH and implication for hypothetical high-pressure form of $Mg(OH)_2$. Physics and Chemistry of Minerals, 31, 360–364.

Kuribayashi, T., Sano-Furukawa, A., and Nagase, T. (2014) Observation of pressure-induced phase transition of δ-AlOOH by using single-crystal synchrotron X-ray diffraction method. Physics and Chemistry of Minerals, 41, 303–312.

Nishi, M., Irifune, T., Tsuchiya, J., Tange, Y., Nishihara, Y., Fujino, K., and Higo, Y. (2014) Stability of hydrous silicate at high pressures and water transport to the deep lower mantle. Nature Geoscience, 7, 224–227.

Oxford Diffraction (2006) CrysAlis RED (Version 1.171.31.2) and ABSPACK in CrysAlis RED. Oxford Diffraction, Abingdon, Oxfordshire, England.

Robinson, K., Gibbs, G.V., and Ribbe, P.H. (1971) Quadratic elongation: a quantitative measure of distortion in coordination polyhedra. Science, 172, 567–570.

Sano-Furukawa, A., Komatsu, K., Vanpeteghem, C.B., and Ohtani, E. (2008) Neutron diffraction study of δ-AlOOH at high-pressure and its implication symmetrization of the hydrogen bond. American Mineralogist, 93, 1558–1567.

Shannon, R.D. (1976) Revised effective ionic radii and systematic studies of interatomic distances in halides and chalcogenides. Acta Crystallographica, A, 32, 751–767.

Sheldrick, G.M. (2008) A short history of SHELX. Acta Crystallographica, A, 64, 112–122.

Shieh, S.R., Mao, H-K., Hemley, R.J., and Ming, L.C. (1998) Decomposition of phase D in the lower mantle and the fate of dense hydrous silicates in subducting slabs. Earth and Planetary Science Letters, 159, 13–23.

Suzuki, A., Ohtani, E., and Kamada, T. (2000) A new hydrous phase δ-AlOOH synthesized at 21 GPa and 1000 °C. Physics and Chemistry of Minerals, 27, 689–693.

Tsuchiya, J. (2013) First principles prediction of a new high-pressure phase of dense hydrous magnesium silicates in the lower mantle. Geophysical Research Letters, 40, 4570–4573.

MANUSCRIPT RECEIVED APRIL 3, 2014
MANUSCRIPT ACCEPTED APRIL 19, 2014
MANUSCRIPT HANDLED BY IAN SWAINSON